KNOT PRODUCTION AND JET DISRUPTION VIA NONLINEAR KELVIN-HELMHOLTZ PINCH INSTABILITIES

Michael L. Norman, Karl-Heinz A. Winkler
Max-Planck-Institut für Physik und Astrophysik
Institut für Astrophysik, Karl-Schwarzschild-Str. 1
8046 Garching b. München, West Germany

L. Smarr*
Departments of Astronomy and Physics, University of Illinois
Urbana, Illinois 60801, USA

ABSTRACT. We summarize the results of time-dependent numerical hydrodynamical simulations which investigate the behavior of pinching modes of the Kelvin-Helmholtz instability in the nonlinear regime. Ordinary mode (OM) pinch instabilities, important only at Mach numbers of order unity, are shown to be disruptive. Reflection mode (RM) pinch instabilities, important in supersonic jets with parameters of astrophysical interest, are shown to be not disruptive, but rather saturate at finite amplitude through the formation of oblique internal shockwaves. The saturated RM pinch instability consists of a near-periodic train of biconical internal shockwaves which propagates with a fraction of the mean flow velocity. Properties of the shock system are given for jets of different density ratios and Mach numbers. The effect of pinch instabilities on energy transport in extragalactic jets is discussed.

1. INTRODUCTION

A persistent worry that has existed since the original proposal of the fluid beam hypothesis (Scheuer, 1974; Blandford & Rees, 1974) to account for the structure and energetics of extragalactic radio sources is the potential disruption of the "energy-pipe" via Kelvin-Helmholtz (K-H) instabilities. Linear stability analyses performed by many authors (e.g. Ferrari et al. 1978, 1981, 1982; Hardee 1979, 1982, 1983; Ray 1981; Cohn 1983) have dealt with this issue, and have generally found that a variety of modes of the K-H instability have significant growth rates even at high Mach numbers. On the basis of linear growth rates, the ordinary mode (OM) helical instability and the reflection mode (RM) pinch instability are potentially the most important modes for flow modification and jet disruption. However, these processes cannot be addressed by a linear analysis, being fundamentally nonlinear.

In this paper we summarize the results of time-dependent numerical hydrodynamical simulations which investigate the behavior of pinching modes in the nonlinear regime. OM pinch instabilities, important only at Mach numbers of order unity, are shown to be disruptive. RM pinch instabilities,

*Visitor, Max-Planck-Institut für Astrophysik; Alfred P. Sloan Fellow

important in supersonic jets with parameters of astrophysical interest (i.e. low density ratio, high Mach number), are shown to be not disruptive, but rather saturate at finite amplitude through the formation of oblique internal shockwaves. The saturated RM pinch instability consists of a near-periodic train of biconical internal shockwaves which propagates with a fraction of the mean flow velocity. The structural and propagation properties of the shock system are given for jets of different beam density ratios and Mach numbers. Growth lengths are determined empirically.

Finally, the role of pinch instabilities in extragalactic jets is discussed. The properties of emission knots produced by the RM pinch instability are deduced using simple synchrotron theory arguments. We show how measurements of knot proper motion can be used to constrain the local flow velocity in pressure-confined supersonic jets.

2. LINEAR PINCH INSTABILITIES

Linear analyses of the K-H instability in supersonic beams distinguish between two basic types of pinch (i.e. axisymmetric) modes depending upon the number of internal nodes in the radial function of the perturbation variables (Ferrari et al. 1981, Cohn 1983). The ordinary, or fundamental, pinch mode has no internal nodes, whereas the reflection modes comprise an infinite family parameterized by the number of internal nodes. Reflection modes derive their name from the special property of a supersonic shear surface investigated by Miles (1957), which is that for certain angles of incidence, a plane linear wave will be reflected from the surface with a greater amplitude than it had upon incidence. A reflection mode instability requires the existence of two such shear surfaces in close proximity, such as in a supersonic beam, between which waves can repeatedly reflect and grow to nonlinear amplitude. In this context, the nodes of a particular reflection mode can be thought of as the point where incident and reflected waves destructively interfere. Thus, whereas the OM is a purely longitudinal mode, the RM posses an additional transverse component.

This difference in physical character is accompanied by differences in linear growth rates and phase and group velocities, which led Cohn (1983) to conclude that the OM and RM dominate in different regions of the density ratio - Mach number parameter space. Defining $\eta = \rho_{beam}/\rho_{external}$, and $M = V_{beam}/C_{beam}$, Cohn determined empirically that the RM have significantly larger growth rates in the regime $M > 2\eta^{0.3}$. This boundary is indicated in Figure 1 by the upper dashed line. The black dots indicate the cases we have studied numerically. As can be seen, we have five cases in the vicinity of this boundary: two on the OM side, and three on the RM side. We can therefore investigate whether there is a change in modal character in the nonlinear regime upon crossing this boundary, and what effect this has on bulk energy transport in supersonic jets.

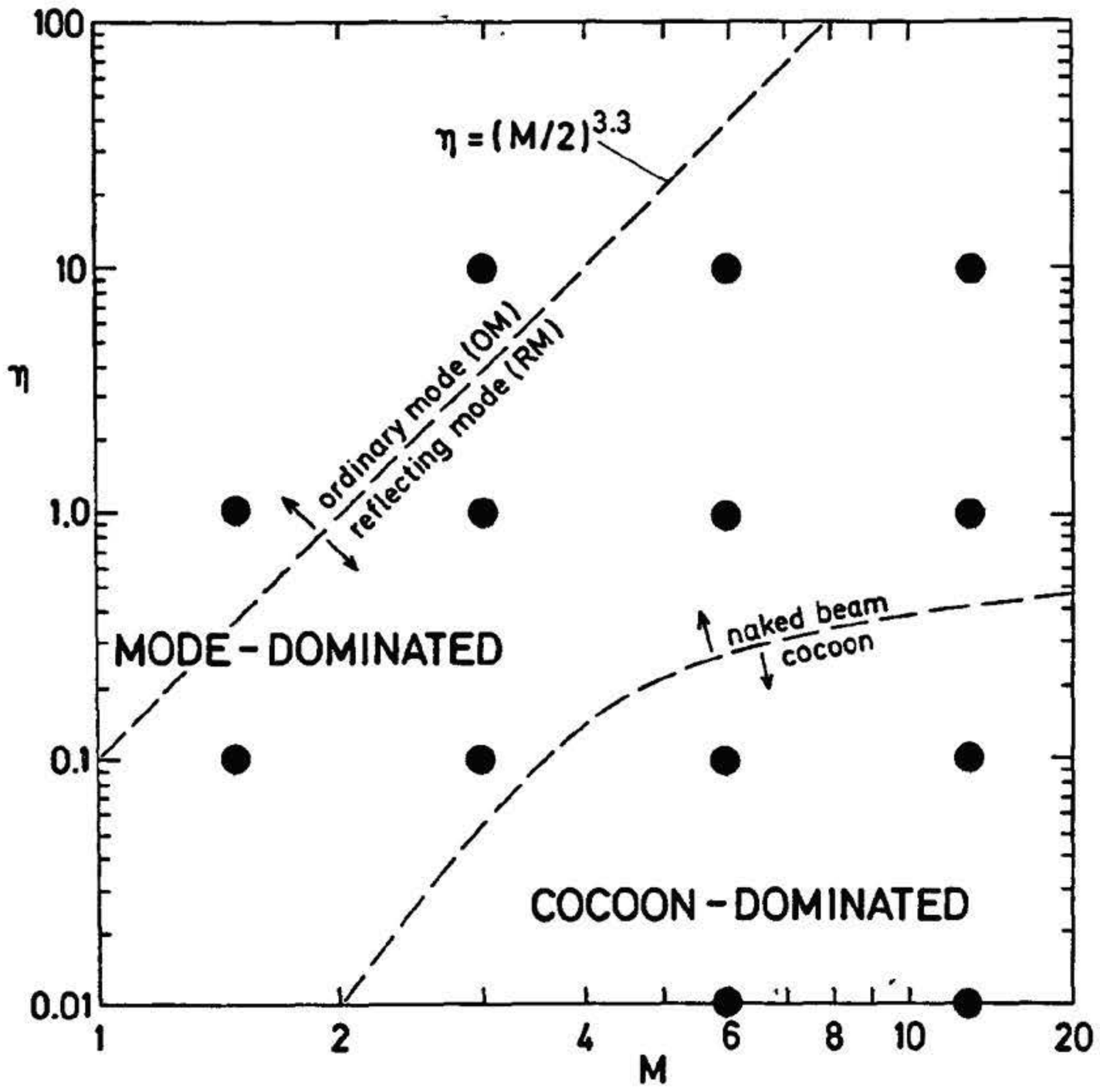


Fig. 1: Structure of parameter space. showing boundaries between ordinary mode-, reflection mode-, and cocoon-dominated regions (dashed lines), and location in parameter space of numerical experiments (black dots), from Cohn (1983), and Norman et al. (1984).

3. JET DISRUPTION

Figure 2 illustrates nonlinear pinch instabilities in the OM-dominated regime. The numerical procedure is as follows. At t = 0, the jet extends across the computational domain $0 \leq R/R_{jet} \leq 10$, $0 \leq Z/R_{jet} \leq 40$, flowing from left to right in pressure equilibrium with the surrounding gas. The initial jet radius is resolved with 20 zones. The jet parameters are $\eta = 10$, $M = 3$. Both jet gas and ambient gas are assumed to obey the ideal gas equation of state with adiabatic index $\gamma = 7/5$. The jet is continuously replenished at left, where a numerical inflow condition has been established; the jet exits the domain at right, where a numerical outflow condition has been established. A perturbation is applied to the jet by adjusting the input sound speed so that the jet flows in with a one percent pressure excess. The subsequent evolution of the jet is computed until a quasi-steady state is reached using the techniques outlined in Norman et al. 1983, and described in detail in Norman and Winkler 1984. The initial jet boundary is kept sharp through the use of the LeBlanc interface tracking technique (Norman 1980; Norman and Winkler, 1984).

In laboratory terminology, we are simulating the downstream behavior of an almost perfectly expanded Mach 3 cold air jet exhausting into a quiescent atmosphere. Experimental data exist for these parameters (Abramovich 1962) with which our numerical results can be compared.

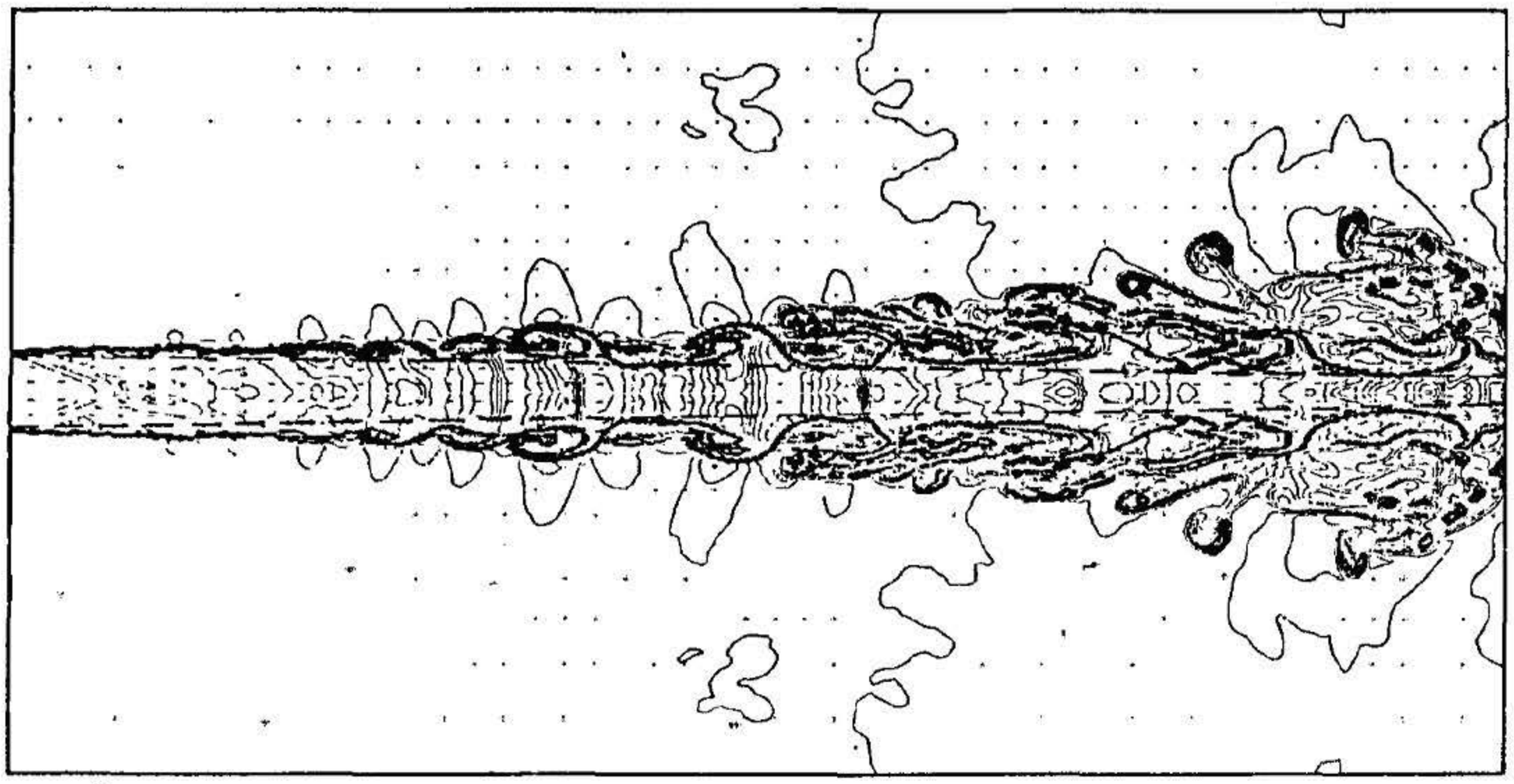


Fig. 2: Nonlinear pinch instability in the OM-dominated regime (M=3, η=10). Density contour plot. Note inward propagation of mixing layer on jet boundary (dashed lines).

Density contours of the flowfield at $\tau \equiv tC_{beam}/R_{beam} = 19$ are shown in Figure 2. The boundary of the jet appears black bocause of the superposition of many contour lines at the 10:1 density discontinuity. The pinch instability manifests itself as waves on the jet boundary, which reach perceptible amplitude roughly five jet diameter downstream of the inlet, and continue to grow in amplitude further downstream. The effect of the instability is to create an ever-broadening mixing layer which eats into the supersonic core of the jet and spreads the jet as a whole. Notice that the inward progress of the mixing layer is governed by long wavelength waves. $\lambda/R_{jet} \geq 1$. We measure a mixing angle for the inner edge of the mixing layer (dashed line in Fig. 2) of $\Theta = \delta/Z \approx -0.02$, where $\delta = R_{edge}-R_{jet}$. Therefore, at $Z \approx 50\ R_{jet}$, the mixing layer will reach the axis, whereupon the jet will become fully turbulent. The rate of outward spreading is more difficult to determine, but appears to be roughly three times the inward spreading rate.

Abramovich (1962) measured supersonic core lengths in various cold air jets, and found a value of $\ell_{core} = 60\ R_{jet}$ for a jet of identical parameters. Insofar as supersonic core lengths in pressure-matched jets in particular are known to be uncertain to 40 to 60% (Shirie and Seubold 1966) - due to the sensitivity of core length on level of input turbulence and precise nozzle geometry - we consider the agreement quite good. A comparison of Mach 1.5 jets is likewise good: the case $\eta = 1$, M = 1.5 described in Norman et al. 1984 (cf. Fig. 10) yields $\ell_{core} \approx 20\ R_{jet}$, whereas Ambramovich measured $\ell_{core} = 19\ R_{jet}$ in the laboratory. We credit the good agreement to the conclusion that the inward progress of the mixing layer is governed by long wavelength shear instabilities, which we <u>can</u> adequately model, and not by short wavelength instabilities, which we <u>cannot</u> adequately model. As the assumption of axisymmetry limits us to studying only poloidal motions, we conclude that poloidal mixing is the dominant mixing process in the first supersonic core-length of the jet.

The flow beyond the terminus of the supersonic core is fully turbulent and subsonic (Shirle and Seubold 1966), and, in effect, disrupted. Unless kept axial by buoyancy or a preferential gradient, the flow will generally not preserve its initial direction. Thus, the role of nonlinear OM pinch instabilities in jets is one of entrainment, decceleration and ultimately disruption, through the establishment of a mixing layer on the jet boundary.

4. KNOT PRODUCTION

Figure 3 illustrates nonlinear pinch instabilities in the RM-dominated regime. The numerical procedure is exactly as described in the last section, only now the jet parameters are $\eta = 1$, $M = 3$. The only change from Figure 2, therefore, is to lower the jet density by a factor of ten. However, the change in flow behavior is striking.

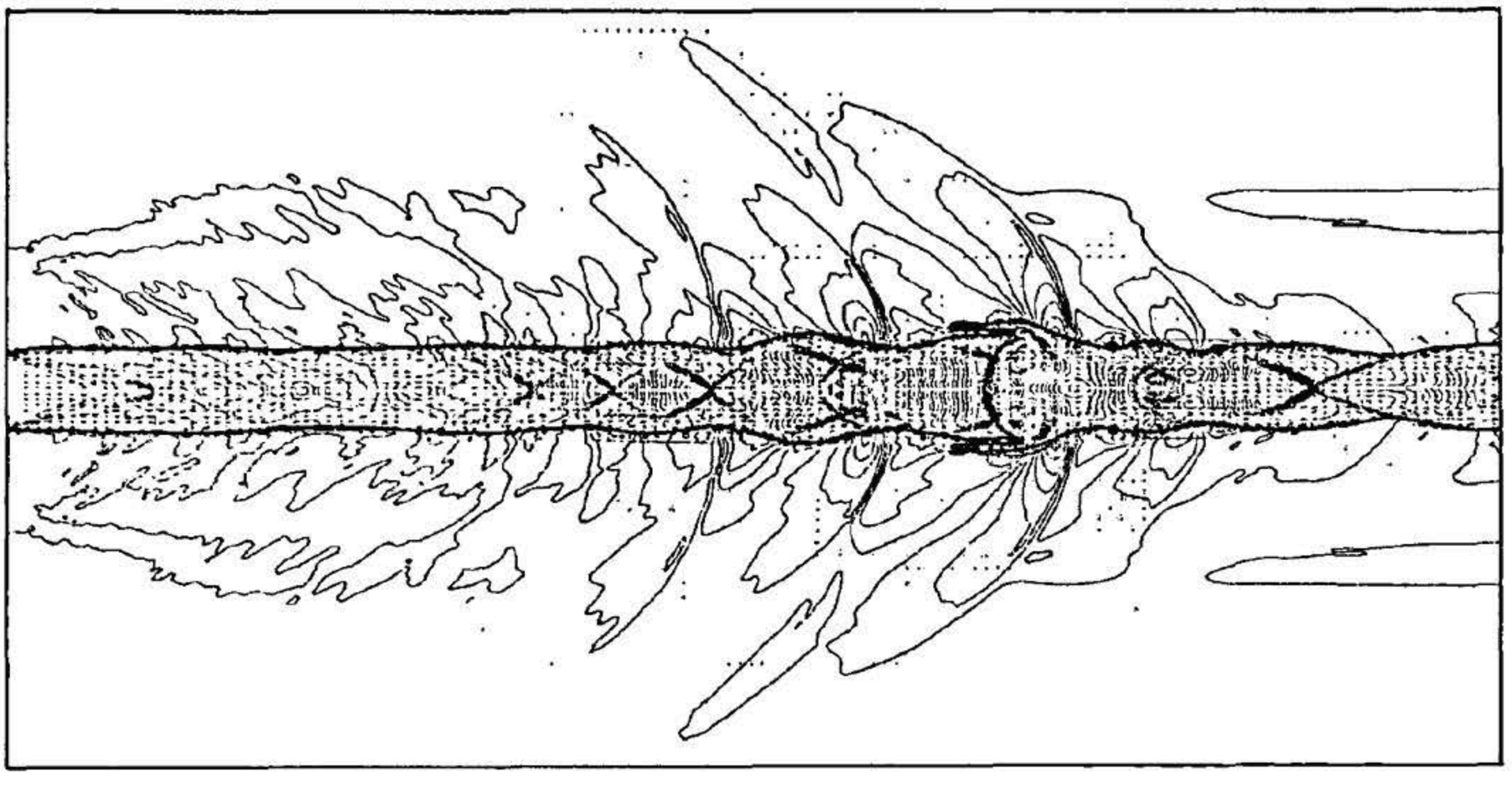


Fig. 3: Nonlinear pinch instability in the RM-dominated regime ($M=3, \eta=1$). Density contour plot. Note undulations of jet boundary (solid lines) and internal and external shockwaves.

Figure 3 shows density contours of the flow field at $\tau = 8$. As the jet and ambient gas have equal densities, the contour lines do not reveal the position of the jet boundary; this is indicated in the Figure by the solid lines. One can see that the jet boundary is no longer subject to turnover and mixing to the extent of that shown in Figure 2, but rather exhibits a finite-amplitude undulation. One can also see the development of oblique shockwaves within the jet, appearing distinctly first at $Z/R_{jet} \approx 11$, and subsequently growing in strength downstream. We observe the positions of shocks and undulations to be coupled, the entire assemblage moving downstream with a substantial fraction of the jet velocity. In the next section we quantify the pattern propagation speed. The pattern propagates supersonically with respect to the ambient medium, and hence the advancing boundary corrugations drive shocks into the surrounding gas. A schematic of the fully-developed flow structure is shown in Figure 4.

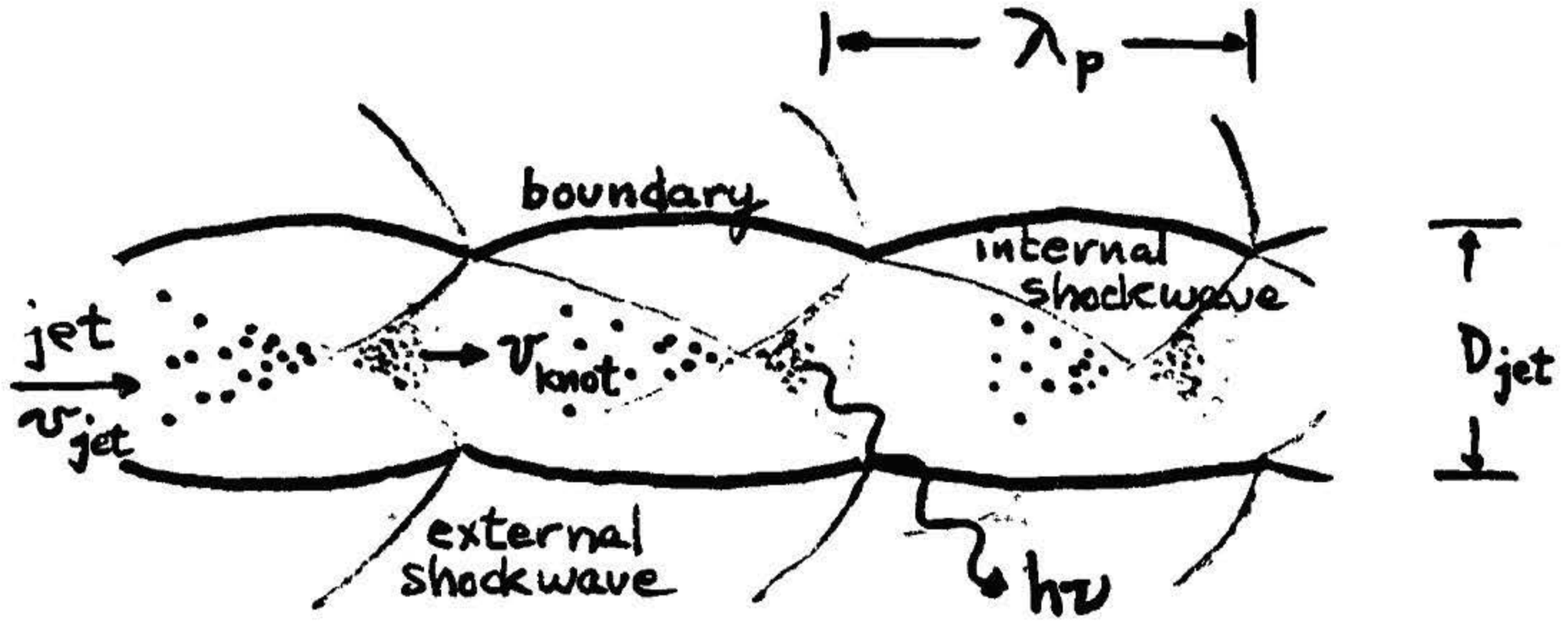


Fig. 4: Schematic of RM-induced shockwaves and high pressure knots, and definition of quantities appearing in Table 1.

The relationship of this nonlinear pinching mode to the linear reflection modes is not entirely clear, although both modes clearly involve the reflection of waves off of the jet boundary to amplify the instability. That both the linear and nonlinear pinch instabilities change character in the same region of the η-M parameter space is compelling evidence for a strong relationship. Insofar as the shockwave system propagates as a coherent unit, it may be a nonlinear superposition of reflection modes, and not a single reflection mode in the nonlinear regime. Figure 3 shows that this is convective instability, with the waveform showing considerable convective evolution. This further complicates a comparison with linear theory.

We can make the following conclusions concerning the effect of this kind of pinch instability on jet energy transport.

The small amount of mixing at the jet boundary in Figure 3 implies that jet deceleration is mediated primarily by the system of internal and external shockwaves. Since the shockwave pattern moves downstream with a substantial fraction of the mean flow velocity and the shockwaves themselves are oblique, they decelerate the mean flow relatively little. These facts point to the conclusion that pinch instabilities in the RM-dominated regime are not disruptive, as in the OM-dominated regime, but rather gradually decelerate the mean flow through the conversion of directed kinetic energy into heat via oblique internal shockwaves. Examples of supersonic jets propagating stably despite extensive arrays of internal shockwaves are given in Norman et al. 1984, Smarr et al. 1984, and in the color plates in the appendix to this paper.

As a consequence of the internal shockwaves produced in the present type of pinch instability, high pressure regions are produced immediately downstream of the points of shock intersection. The possibility that these regions may be observed as emission knots in astrophysical jets is discussed in Norman et al. 1984, and in the last section of this paper. Here we simply point out that emission knots thus produced would exhibit the characteristic spacing and propagation velocity of the underlying shock system. It is therefore important to determine how these quantities depend on jet parameters, so that observations of knot spacing and proper motion can be used as a probe of the underlying flow.

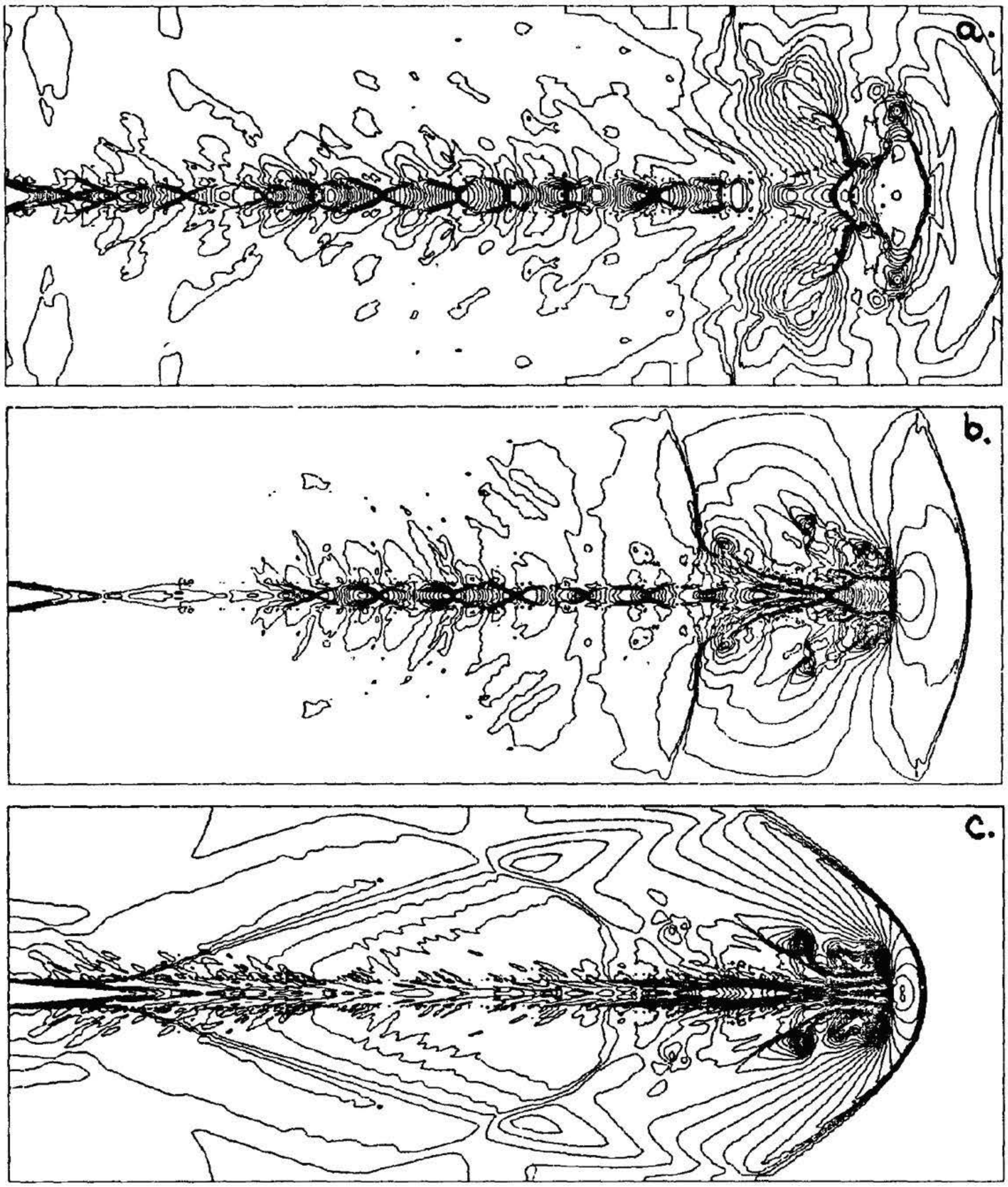


Fig. 5: Pressure contour plots showing shockwave structure in pressure-matched jets of varying Mach numbers and density ratios. a) M=3, η=1; b) M=6, η=10; c) M=12, η=10. Note Mach number dependence of distance from inlet to the first strong internal shockwave.

5. NONLINEAR PROPERTIES

Returning to Figure 1, we see that the majority of our data points lie below the line $M = 2\eta^{0.3}$, in the RM-dominated region of parameter space. This is also likely to be the region of greatest astrophysical relevance. In this section we discuss the occurrence and nonlinear properties of pinch instabilities in the RM-dominated regime in order to investigate their dependence on jet density ratio and Mach number. The calculational data base we shall use for this investigation are the set of propagating jets described and documented in Norman et al. 1983 and in the appendix to this paper.

Of the eleven cases satisfying $M > 2\eta^{0.3}$ in Figure 1, only seven are suitable for our purposes; the jets with parameters lying below the lower dashed line in Figure 1 exhibit internal shock structures that are driven by perturbations in the surrounding cocoon ("cocoon-dominated", see Norman et al. 1984). The jets of the seven remaining cases have essentially no cocoons ("naked beam"), and several exhibit shock structures which are ordered ("mode-dominated"). The parameters of the seven jets considered are listed in Table 1. Snapshots of the flowfields at advanced times are presented in the appendix.

5.1 Occurrence and Growth length

In all but Case 2 and Case 10 of Table 1, we find regular arrays of biconical shockwaves arise in the flow. At Mach 1.5 the instability is either not excited or the shockwaves are too weak to be detected. By Mach 3, the shock systems are prominent and extensive (cf. Fig. 5a). At Mach 6 we observe that the shock system develops further downstream (cf. Fig. 5b), although it is quite similar in appearance to the Mach 3 shock system once fully developed. Further increasing the Mach number to 12 shows that there is clearly a Mach number scaling of the pinch instability growth length, as internal shockwaves are largely absent in the first 24 jet diameters downstream of the inlet (cf. Fig. 5c). However, when the jet in Figure 5c is allowed to propagate to greater lengths, as in Figure 6, boundary constrictions and the accompanying shockwaves do emerge further downstream.

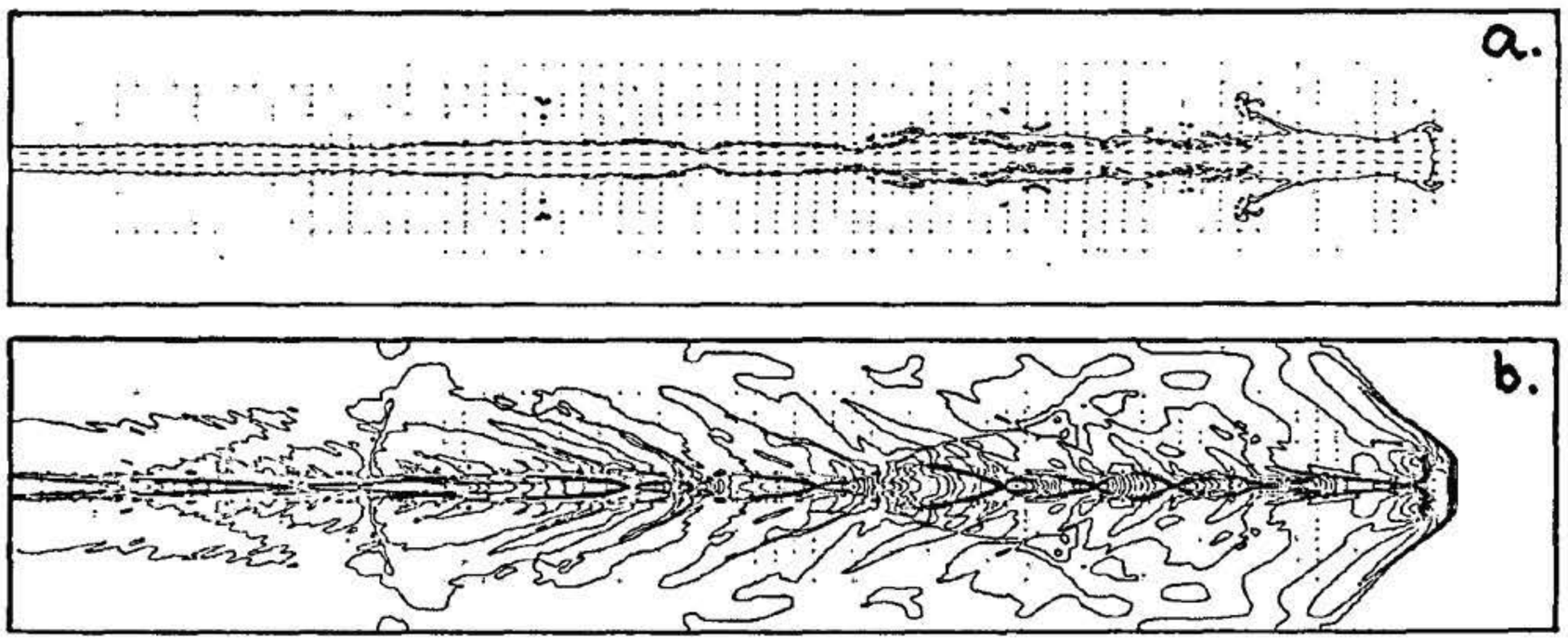


Fig. 6: Development of RM pinch instability in a high Mach number jet (M=12, η=10). a) jet boundary, showing undulations; b) pressure contour plot, showing shock structure.

TABLE 1. Shockwave pattern wavelength and propagation speed

Case*	M	η	λ_p / R_{jet}	V_p	V_p / V_{jet}	$M - \frac{V_p}{c_{jet}}$	$\frac{p_{knot}}{p_{ambient}}$	comments
2	1.5	0.1	-	-	-	-	-	no shock system
3	3.0	1.0	4.8	0.8	0.25	2.2	2.	well-developed shock system
4	3.0	0.1	4.8	1.4	0.14	2.6	3.	well-developed shock system
5	6.0	10.	5.0	1.0	0.53	2.8	3.	well-developed shock system
6	6.0	1.0	5.2	2.5	0.42	3.5	4.	boundary effects
9+	12.0	10.	≥ 9.5	≤ 2.5	≤ 0.66	≥ 4.1	5.	convective evolution
10	12.0	1.	-	-	-	-	-	no shock system-insufficient length

Case numbers according to Table 2, Appendix
extended domain $0 \leq Z \leq 160$, cf. Fig. 6

Our numerical results are consistent with a linear scaling of instability growth length with Mach number $\ell_g = \alpha M D_{jet}$ with $1 \leq \alpha \leq 2$. Physically, this means that only one or two wave reflections are needed to amplify the perturbations applied to the jet at the inlet to nonlinear amplitude.

5.2 Wavelength and pattern speed

Table 1 summarizes pattern wavelength λ_p and propagation speed V_p for those cases where the shockwave system is well-developed. The wavelength assumes a typical value of $\lambda_p / R_{jet} \approx 5$ in the range $3 \leq M \leq 6$, with a weak Mach number dependence. Case 9 shows convective evolution of the shock pattern wavelength $\frac{d\lambda_p}{dZ} < 0$ (cf. Fig. 6b), and thus only a lower limit on λ_p is indicated.

Normalized pattern velocities V_p / V_{jet} show positive dependencies on density ratio and Mach number. The relative Mach number of the jet with respect to the pattern $M - V_p / C_{jet}$ is also tabulated, and accordingly shows a negative dependence on density ratio and a positive dependence on Mach number.

5.3 Knot overpressure

Typical (not peak) values of knot overpressure $P_{knot} / P_{ambient}$ are shown in Table 1, and show a positive dependence on the relative Mach number defined above. That the dependence is not quadratic could be due to shock obliquity.

Although Case 6 develops strong internal shockwaves, a spurious wave which is generated where the bow shock encounters the R = 15 boundary impinges on the jet, and perturbs it considerably. The shock system is likely to have been driven by this perturbation, or at least modified by it. Therefore, the entries in Table 1 under Case 6 are less reliable than the others.

Case 10 does not develop an extensive internal shock system, presumably because the domain was too short to allow the pinch-instability to grow.

6. ASTROPHYSICAL IMPLICATIONS

Kelvin-Helmholtz instabilities couple a supersonic jet to its confining medium via mass and momentum exchange. In general, the rate of this exchange depends upon the properties of the two media and the nature of the excited mode(s), and governs the efficiency of streamwise energy transport within the jet. Pinch instabilities allow a high degree of coupling in principle because the wavefronts of all unstable modes are normal to the flow direction, thus maximizing the rate of momentum transfer from the jet to its environment.

We have confirmed the result of Cohn (1983) that pinch instabilities change character across the boundary given by $M=2\eta^{0.3}$. Jets satisfying $M<2\eta^{0.3}$ lie in the ordinary mode-dominated regime, and couple to their environment primarily via mass exchange in a mixing layer at the jet boundary. Jets satisfying $M>2\eta^{0.3}$ lie in the reflection mode-dominated regime, and couple to their environment via shockwaves, which transfer jet momentum directly without mass exchange. With regard to energy transport, OM-dominated jets are more severly effected than RM-dominated jets, the former being subject to deceleration and disruption via entrainment and mixing, while the latter propagate without disruption despite some dissipation of directed kinetic energy at internal shockwaves.

This bimodal behavior of how pinch instabilities effect jet kinetic energy transport may help explain the correlation between radio power and morphological class in extended double radio sources (Fanaroff and Riley, 1974). Assuming that the integrated radio power of a source is a measure of the kinetic power of the jet supplying it, then low power sources will have jets in the OM-dominated regime and hilgh power sources will have jets in the RM-dominated regime, since the jet kinetic luminosity $\mathcal{L}_{jet} \propto M^3\eta^{-\frac{1}{2}}$. It is important to note that virtually all laboratory supersonic jets lie in the OM-dominated regime, as they are dense and cold ($\eta > 1$) and of low Mach number ($M \leq 3.5$). As we have seen in Section 3, such jets develop turbulent boundary layers which ultimately consume the supersonic core, and become thereafter fully turbulent. Jets powering "relaxed" doubles may therefore <u>look</u> like laboratory jets because they <u>are</u> like laboratory jets insofar as they are fully turbulent. The effects of pressure stratifications in the interstellar and intergalactic medium confining the radio jet may limit the usefulness of laboratory analogies, however.

As we have seen in Section 4, internal shockwaves are the distinguishing characteristic of jets in the RM-dominated regime, provided that

the jet length sufficiently exceeds the instability growth length. If RM pinch instabilites were the dominant energy dissipation mechanism in high power radio -jets, then their distinguishing morphological feature would be moving emission knots. However, since the instability growth length scales linearly with Mach number, and jet power scales with the cube of the Mach number, the highest power jets may not produce emission knots, and may be effectively invisible.

Typical knot overpressures are less than an order of magnitude (cf. Table 1), although knot-interknot pressure ratios are considerably greater, due to the strong rarefaction zones which precede the internal shockwaves. A factor of ten pressure variation is common in RM-dominated jets (cf. Fig. 10a, Smarr et al. 1984), which would yield a factor of $\sim 10^2$ in radio brightness, assuming that the synchrotron emissivity scales with roughly the square of the particle energy density (Smith et al., 1984).

Knots propagate downstream with 10-50% of the jet speed (cf. Table 1); measurements of knot proper motion would therefore constrain the jet speed to lie within the range $2 \leq V_{jet}/V_{knot} \leq 10$.

Little experimental data exists on jets in the RM-dominated regime, where the jets which power the edge-brightened radio sources most certainly lie. L. Mach (1897) describes an experiment where he produced a supersonic jet of roughly one centimeter in diameter, and one meter in length, the first thirty centimeters of which had no apparent mixing layer. The jet's parameters put it just into the RM regime, which could account for the enhanced boundary stability. Experimental verification of the reflection mode pinch instability and the propagating shock system it produces would be an extremely important test of the explanation of radio source morphology given above, as well as our emission knot mechanism. Begelman, Blandford, and Rees (1984) review the experimental prospects for exploring this low density, high Mach number regime.

Finally, a jet propagating in a non-constant and stratified atmosphere, such as exists in and around elliptical galaxies, is subject to "parameter evolution"; that is, the jet's Mach number and density ratio are no longer constant parameters, but vary as a function of position down the jet. This topic is pursued by Sumi and Smarr in a paper in these proceedings. As Sumi and Smarr show, parameter evolution is relatively slow for jets in isothermal atmospheres, which means that a jet is either in the OM or the RM regime along its entire length, and therefore has the corresponding stability and energy transport properties. Jets in cooling-core accretion flows, however, are subject to rapid parameter evolution, which Sumi and Smarr show is one of increasing density ratio at approximately constant Mach number. The significance of this is that a jet with initial parameters in the RM regime will evolve into the OM regime and be disrupted. Physically, this occurs because the external sound speed is an increasing function of galactocentric distance and the jet Mach number with respect to the confining ambient gas drops below unity.

Sumi and Smarr propose that the wide-angle tail (WAT) morphology is a consequence of local jet disruption via rapid parameter evolution, with the inner collimated jet being in the RM regime and the outer plume-like

structure being in the OM regime. If this model proves correct, then observations of WAT jet morphology could provide information on the distribution of the gaseous environment in which they propagate. Conversely, a knowledge of pressure and temperature distributions around galaxies, used in conjuction with theoretical and numerical jet models, could provide useful constraints on the physical properties of the jet.

ACKNOWLEDGEMENTS

L. S. acknowledges partial financial support under NSF grants nos. PHY 80-01496 and 83-08826.

REFERENCES

Abramovich, G. N. 1962, "Theory of Turbulent Jets", (Gosudarstvennoye Izdatel stvo Moscow, 1960); English translation by the U. S. Air Force Systems Command, Foreign Tech. Div., Technical Documents Liaison Office, MCL 3256, ASTIA AD 283, 858 (1962).

Blandford, R. D., & Rees, M. J. 1974, M. N. R. A. S., 169, 395.

Begelman, M. C., Blandford, R. D., & Rees, M. J. 1984, Rev. Mod. Phys., 26, 255.

Cohn, H. 1983, Ap. J. 266, 73.

Fanaroff, B., & Riley, J. M. 1974, M. N. R. A. S., 167, 31.

Ferrari, A., Trussoni, E., & Zaninetti, L. 1978, Astr. Ap., 64, 43.

Ferrari, A., Trussoni, E., & Zaninetti, L. 1981, M. N. R. A. S. 196, 1054.

Ferrari, A., Trussoni, E., & Zaninetti, L. 1982, M. N. R. A. S. 198, 1065.

Hardee, P. E. 1979, Ap. J., 234, 47.

Hardee, P. E. 1982, Ap. J., 257, 509.

Hardee, P. E. 1983, Ap. J., 269, 94.

Mach, L. 1897, Wien Ber., 106-II, 1025.

Miles, J. W. 1957, J. Acous. Soc. Amer., 29, 226.

Norman, M. L. 1980, Ph. D. dissertation, University of California at Davis; Lawrence Livermore Laboratory Report UCRL-52946.

Norman, M. L., Winkler, K.-H. A., & Smarr, L. L. 1983, in "Astrophysical Jets", ed. A. Ferrari & A. G. Pacholczyk, (Dordrecht: Reidel).

Norman, M. L., Smarr, L. L., & Winkler, K.-H. A. 1984, in "Numerical Astrophysics: A Festschrift in Honor of James R. Wilson", ed. R. Bowers, J. Centrella, J. LeBlanc, & M. LeBlanc, (Jones and Bartlett: Boston).

Norman, M. L., & Winkler, K.-H. A. 1984, in preparation.

Ray, T. P. 1981, M. N. R. A. S., 196, 195.

Scheuer, P. A. G. 1974, M. N. R. A. S., 166, 513.

Shirie, J. W., & Seubold, J. G. 1966, AIAA Journal, 5, 11, 2062.

Smarr, L. L., Norman, M. L., & Winkler, K.-H. A. 1984, Physica D. In press.

Smith, M. D., Norman, M. L., Winkler K.-H. A., & Smarr, L. L. 1984, submitted M. N. R. A. S.

Winkler, K.-H. A., & Norman, M. L. 1984, in preparation.

APPENDIX:
Shock structure, strength, and history in pressure-matched supersonic jets.

In this appendix, color plates*are presented which display shockwave-related phenomena in the parameter survey of jets introduced in Norman et al. 1983, and discussed in Norman et al. 1984, Smarr et al. 1984 and the present paper. These plates are intended to complete the archive begun in Norman et al. 1983 (cf. Sect. 3) displaying properties of our jet survey.

As discussed in Norman et al. 1984, shockwave behavior in pressure-matched jets is sensitive to the two input parameters of Mach number $M \equiv V_{jet}/C_{jet}$ and density ratio $\eta \equiv \rho_{jet}/\rho_{ambient}$. A key factor in this sensitivity is whether or not the jet builds a cocoon around it as it propagates, for a jet with a cocoon is a) effectively propagating in a medium with different properties than the true ambient medium, and b) shockwaves can be driven by motions within the cocoon. Plate 1 illustrates the variations in cocoon thickness and extent as density ratio is varied by three orders of magnitude in four Mach 12 jets; from top to bottom, the density ratios are η = 10., 1., 0.1, and 0.01.

The 73 colors shown in the color bar at the bottom of Plate 1 are each assigned to a particular value of the gas density such that the highest density regions are bright red, the lowest density regions are dark blue, and intermediate values of density in equal logarithmic intervals are assigned the spectral colors in between. Thus, our color bar spans the entire dynamic range of the physical quantity being plotted. Since our grid has 640 zones along the axis of symmetry, while the color image has only 512 pixels, the image slightly underresolves our solution. As the calculations are axisymmetric, the image has been mirrored about the axis of symmetry for ease of visualization.

The remaining twelve Plates each display a jet of a particular parameter pair, using three different flow visualization techniques that we find useful in studying the structure, strength and evolution of shockwaves in time-dependent jets. The format is as follows.

The top frame shows shockwaves and strong compression and rarefaction zones that develop in the flow. Operationally what is done is to assign to each computational zone a color depending on the sign and magnitude of the local divergence of the velocity field $\underline{\nabla}\cdot\underline{V}$. Large negative divergences pick out shockwaves and compression zones, which are colored red; large positive divergences pick out expansion zones, which are colored blue. Any zone that is less than 5% of the largest positive $\underline{\nabla}\cdot\underline{V}$ in the flow, and greater than 5% of the smallest negative $\underline{\nabla}\cdot\underline{V}$ in the flow is colored white. Other parts of the jet/ambient medium are assigned grey tones as follows: black-jet boundary (contact discontinuity), light grey - disturbed ambient medium, and dark grey - undisturbed ambient medium.

The middle frame is a seventy-three color representation of the gas pressure distribution in the flow, made in precisely the same way as described above for the density plots in Plate 1. The color bar is the same as shown in Plate 1.

*Reproduced here in black-and-white. For color presentation, see Report MPA 151 of the Max-Planck-Institut für Astrophysik (September 1984), available on request from the authors.

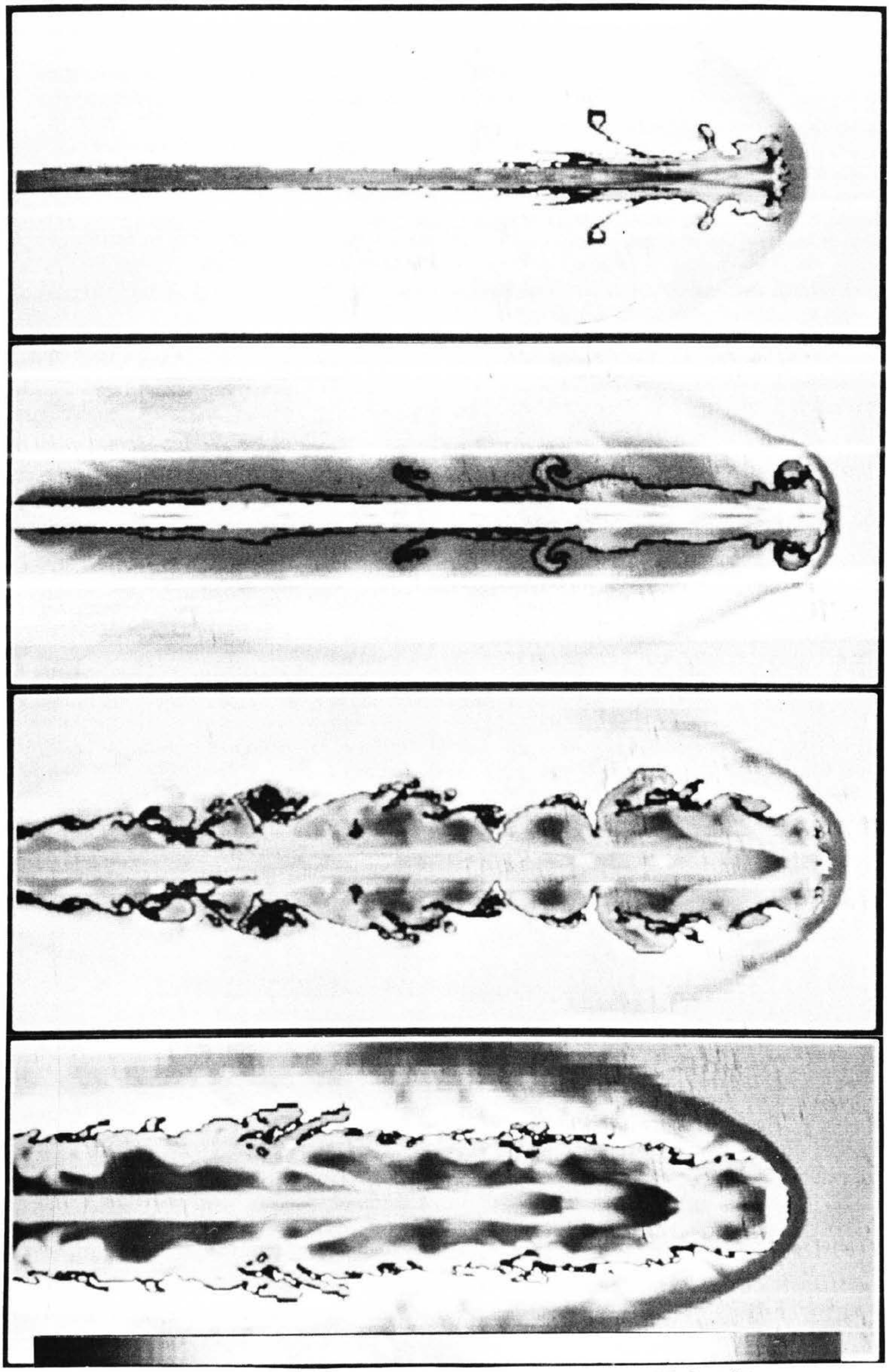


Plate 1. Dependence of cocoon thickness on beam density for four Mach 12 jets

The bottom frame shows the space–time history of the gas pressure on the axis of the jet, and indirectly records a great deal about shock dynamics in a propagating jet. The space–time "grid" consists of 640 by (typically) 300 uniform zones, with the space axis running horizontally $0 \leq Z \leq 80$, and the time axis running vertically $t_1 \leq t \leq t_2$; t_1 and t_2 are given in Table 2. Operationally, the procedure is the same as in the middle frame, however here only 15 bins are used between the minimum and maximum pressures. To further enhance the high pressure regions, all pressure bins below and including ambient pressure have been assigned the grey tones shown in the accompanying color bars. The color bars used in conjuction with the maximum and minimum pressures and pressure increments given in Table 2 allow one to derive quantitative information from the color figures, such as the mean knot overpressure discussed in Section 5, above.

Further details on how these plots are physically made, as well as an efficient algorithm for generating them are given in Winkler and Norman 1984.

CAPTION FOR PLATES 2–13:

Shock structure, strength, and history in pressure–matched supersonic jets. Top frame: composite jet structure showing shockwaves and strong compression zones (bright red), strong rarefaction zones (dark blue), jet gas (white), unshocked external gas (dark grey), shocked external gas (light grey), and contact discontinuity (black). Middle frame: false color image of the logarithm of the gas pressure, where maximum pressure is red, minimum pressure is blue, and intermediate pressures are assigned the spectral colors of the color bar in Plate 1. Bottom frame: false color image of the axial pressure as a function of space (horizontal axis) and time (vertical axis). Color bar and Table 2 define the pressure levels; pressure levels below and including ambient pressure are given in grey tones. See text for further information.

TABLE 2. Physical data for space–time axial pressure plots in Plates 2–13

Case	M	η	t_1	t_2	P^*_{min}	P^*_{max}	P_{n+1}/P_n †	Comments
1	1.5	1.0	10.	187.	2.3(−1)	2.8	1.19	substantial entrainment
2	1.5	0.1	5.	120.	1.4(−1)	3.2	1.25	little entrainment
3	3.0	1.0	4.	118.	1.7(−2)	4.0	1.47	propagating knots modulated by standing oscillation: $\lambda/R \approx 9.5$
4	3.0	0.1	1.	60.	1.5(−2)	7.5	1.56	complex transition to ordered knot phase: $t \geq 40$.
5	6.0	10.	2.5	80.	1.8(−2)	7.0	1.52	strong trailing shockwave; knots
6	6.0	1.0	2.5	43.5	2.0(−2)	1.1(1)	1.57	knots excited by spurious reflected shockwave
7	6.0	0.1	1.	27.	9.2(−3)	3.5(1)	1.80	cocoon–driven internal shockwaves: $\frac{dz}{dt} \approx -2$.
8	6.0	0.01	1.	28.	1.4(−2)	9.2(1)	1.90	short–timescale pressure fluctuations
9	12.0	10.	2.	38.	2.7(−2)	1.3(1)	1.55	quasi–ballistic jet; scant internal structure despite spurious impinging shockwave
10	12.0	1.0	1.25	20.	5.2(−2)	6.5(1)	1.67	thin cocoon; shear–wave induced internal shocks near jet terminus
11	12.0	0.1	0.5	14.	1.0(−2)	3.2(2)	2.10	cocoon–driven internal shockwaves
12	12.0	0.01	1.	7.6	1.8(−2)	5.0(2)	2.10	strong pressure variations near jet terminus

*normalized by the ambient pressure
†pressure ratio between color bar levels in space–time axial pressure plots

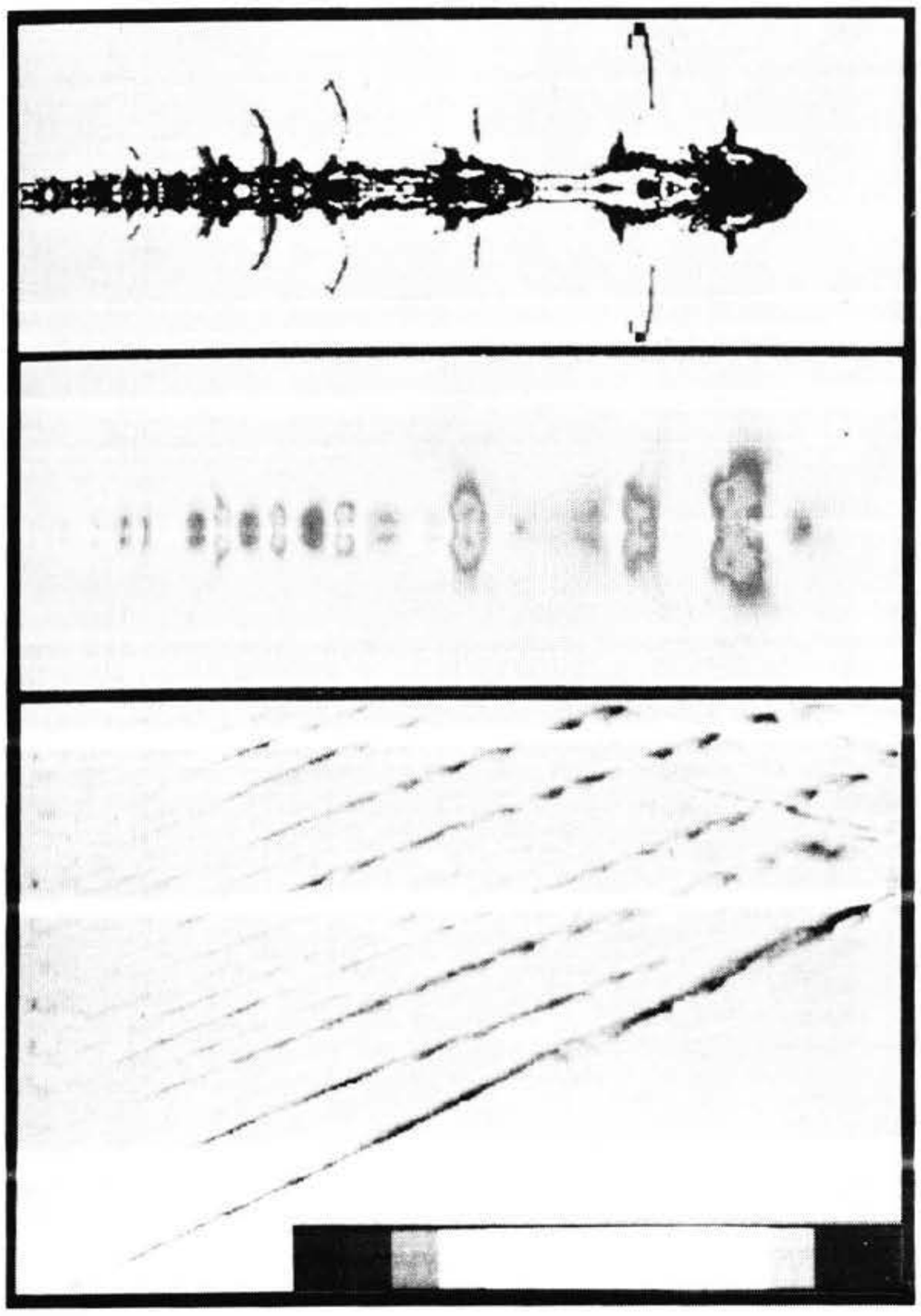


Plate 2. Density Ratio = 1, Mach Number = 1.5

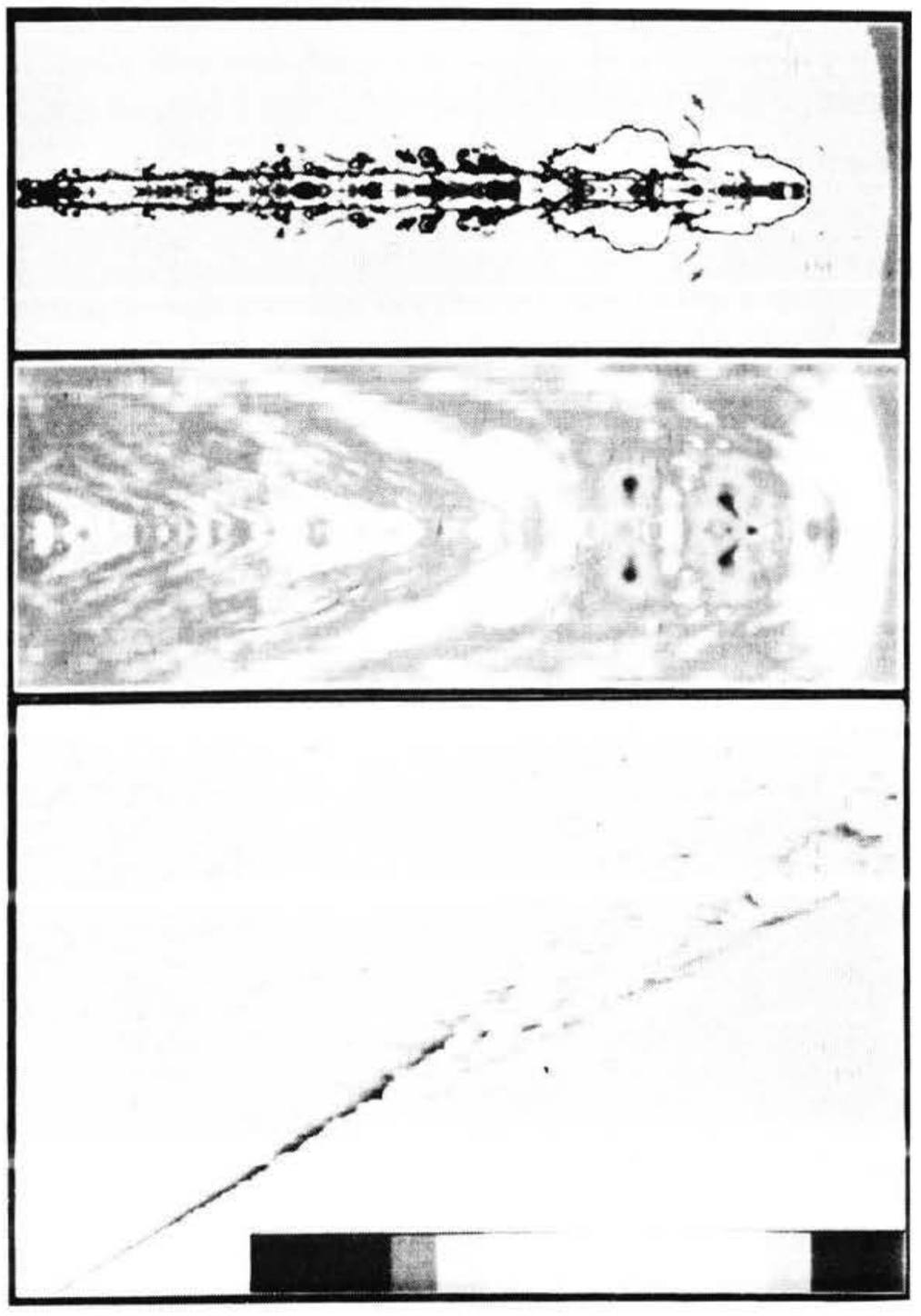


Plate 3. Density Ratio = 0.1, Mach Number = 1.5

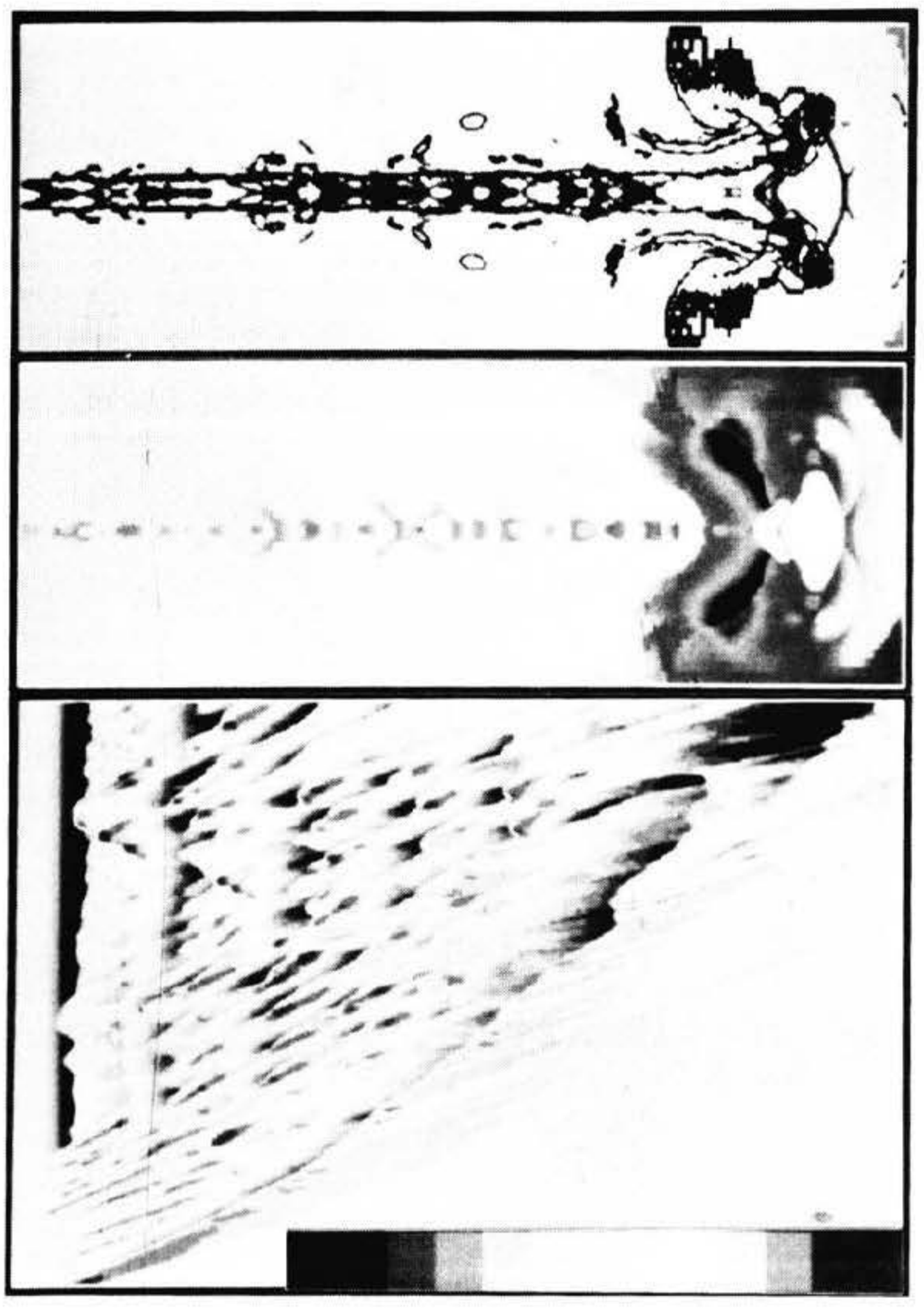


Plate 4. Density Ratio = 1, Mach Number = 3

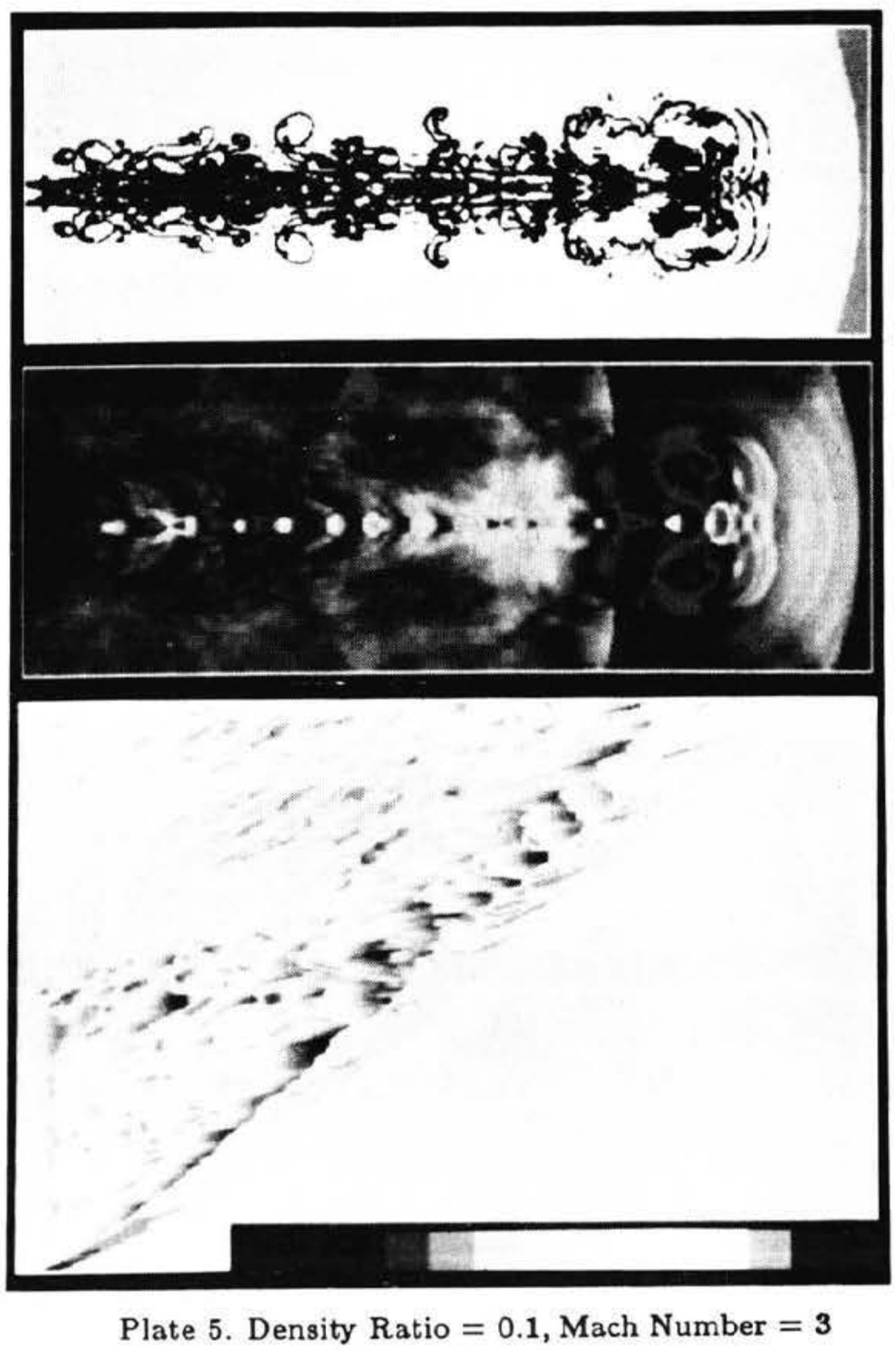


Plate 5. Density Ratio = 0.1, Mach Number = 3

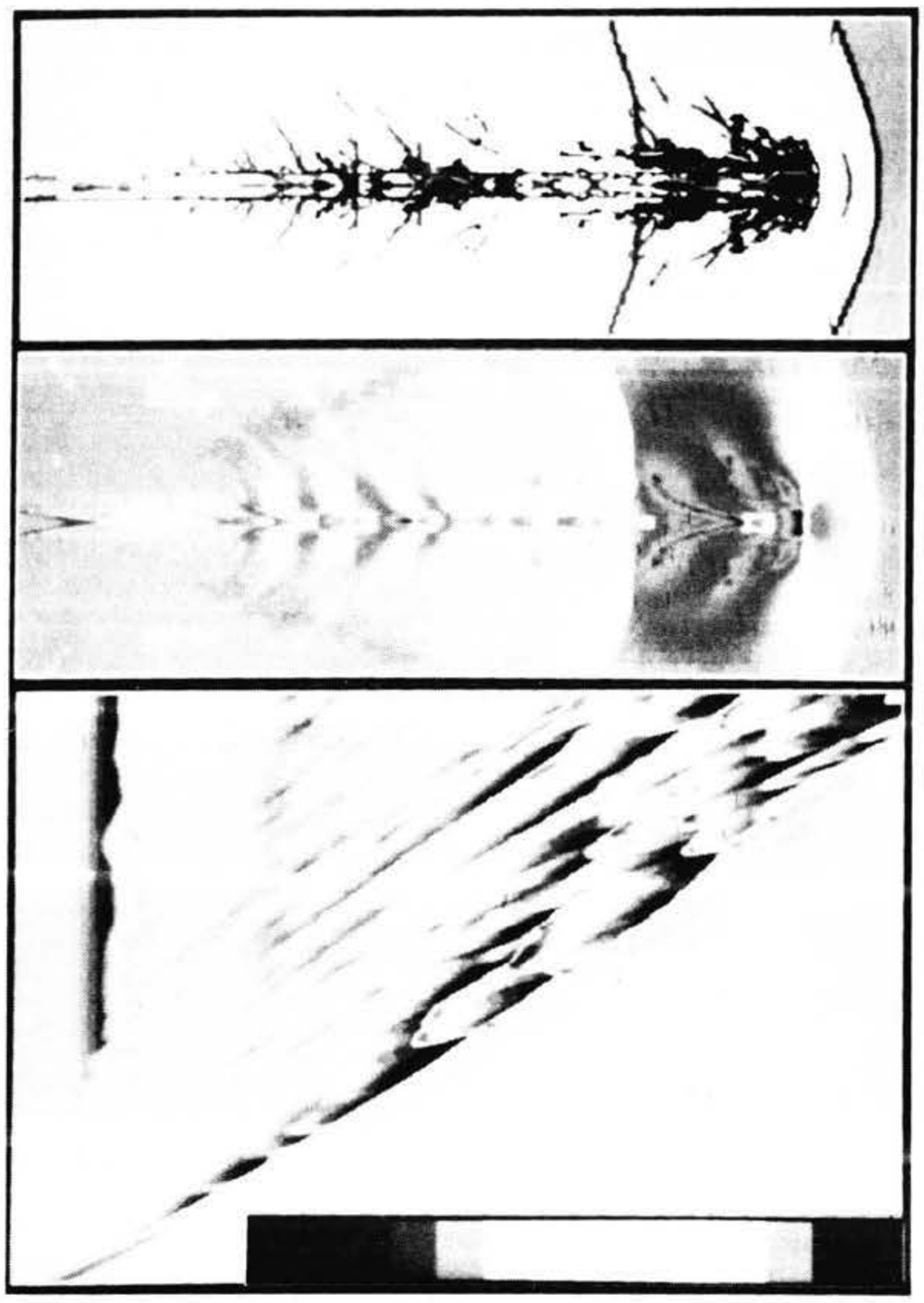


Plate 6. Density Ratio = 10, Mach Number = 6

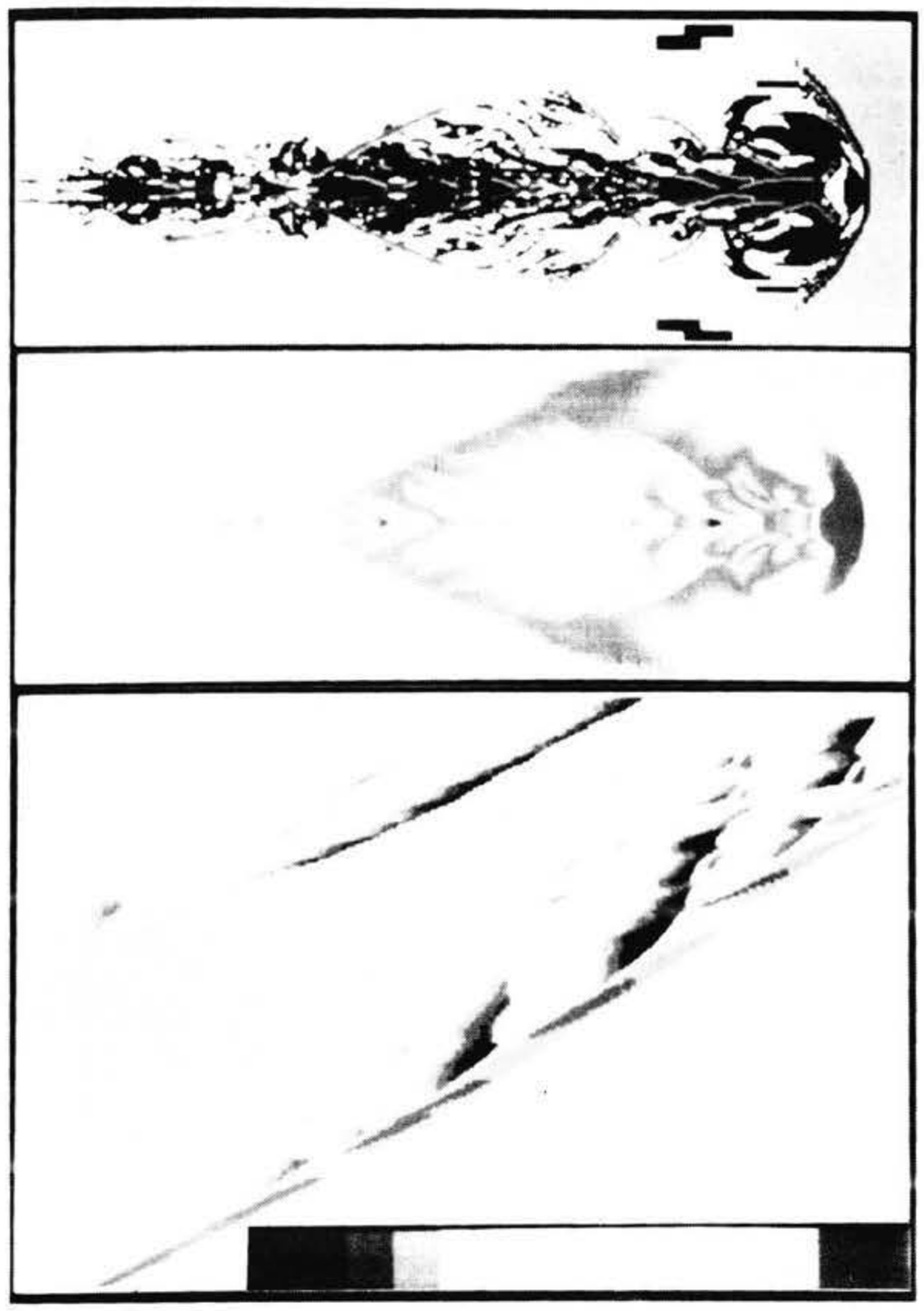


Plate 7. Density Ratio = 1, Mach Number = 6

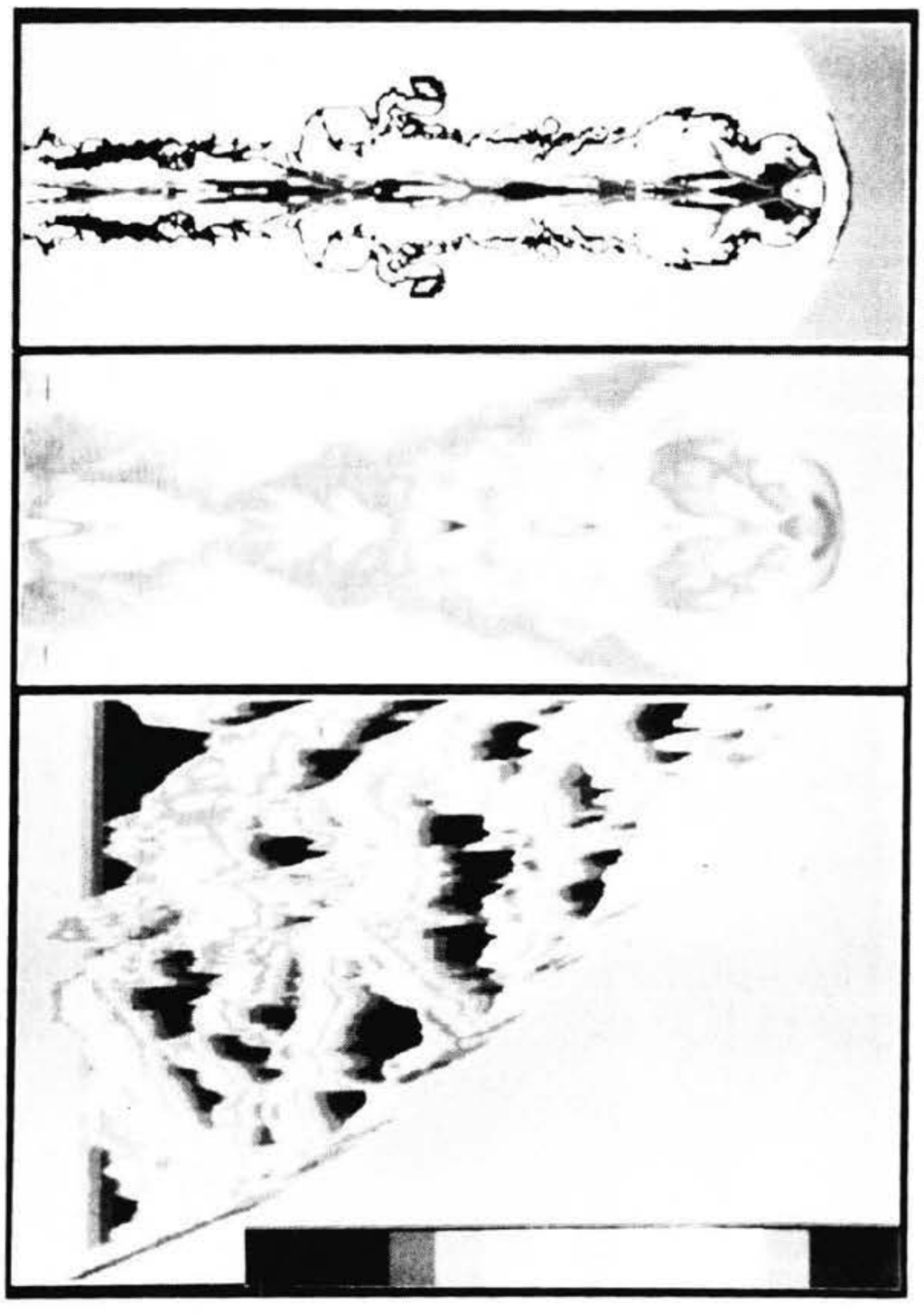


Plate 8. Density Ratio = 0.1, Mach Number = 6

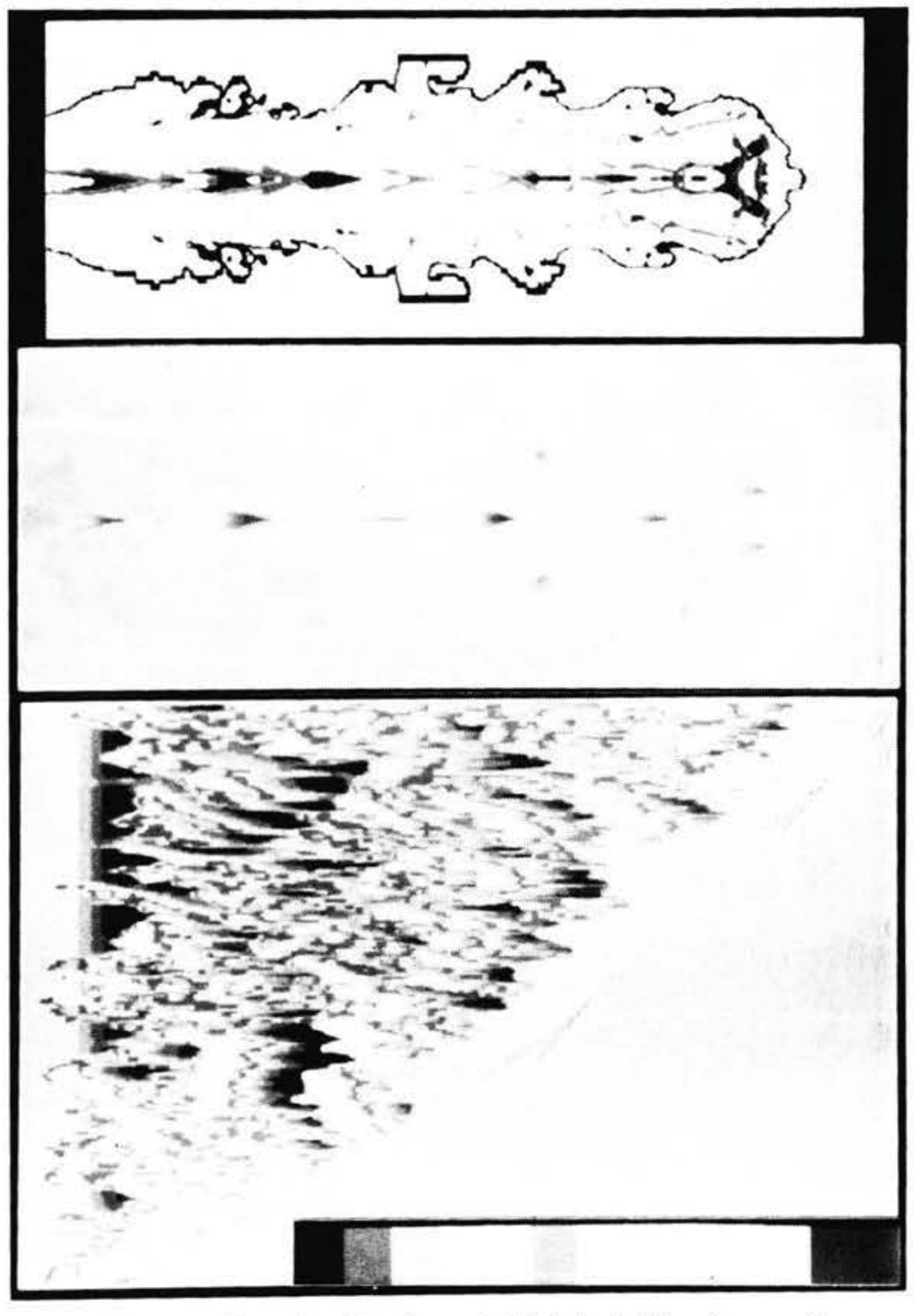


Plate 9. Density Ratio = 0.01, Mach Number = 6

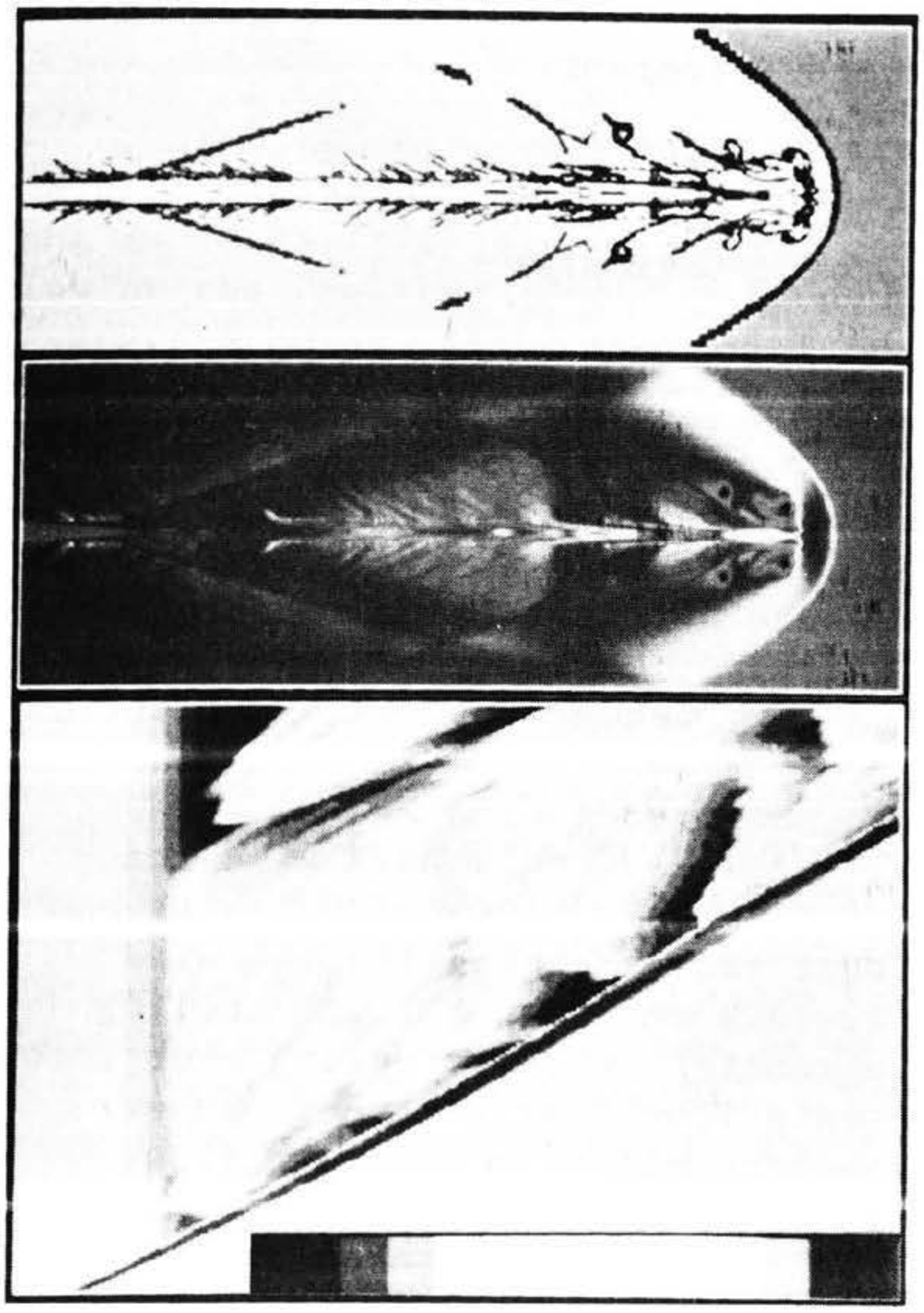


Plate 10. Density Ratio = 10, Mach Number = 12

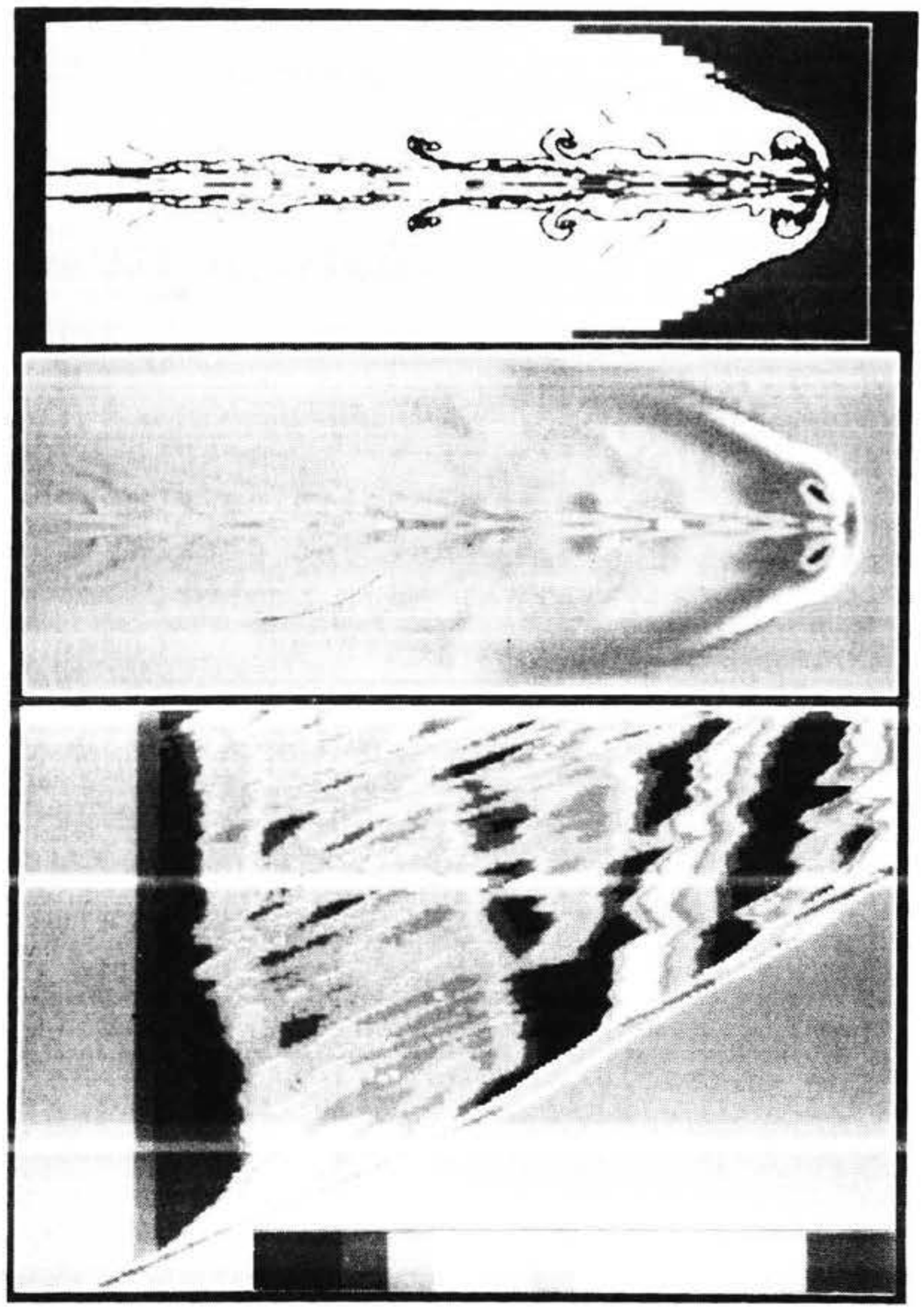


Plate 11. Density Ratio = 1, Mach Number = 12

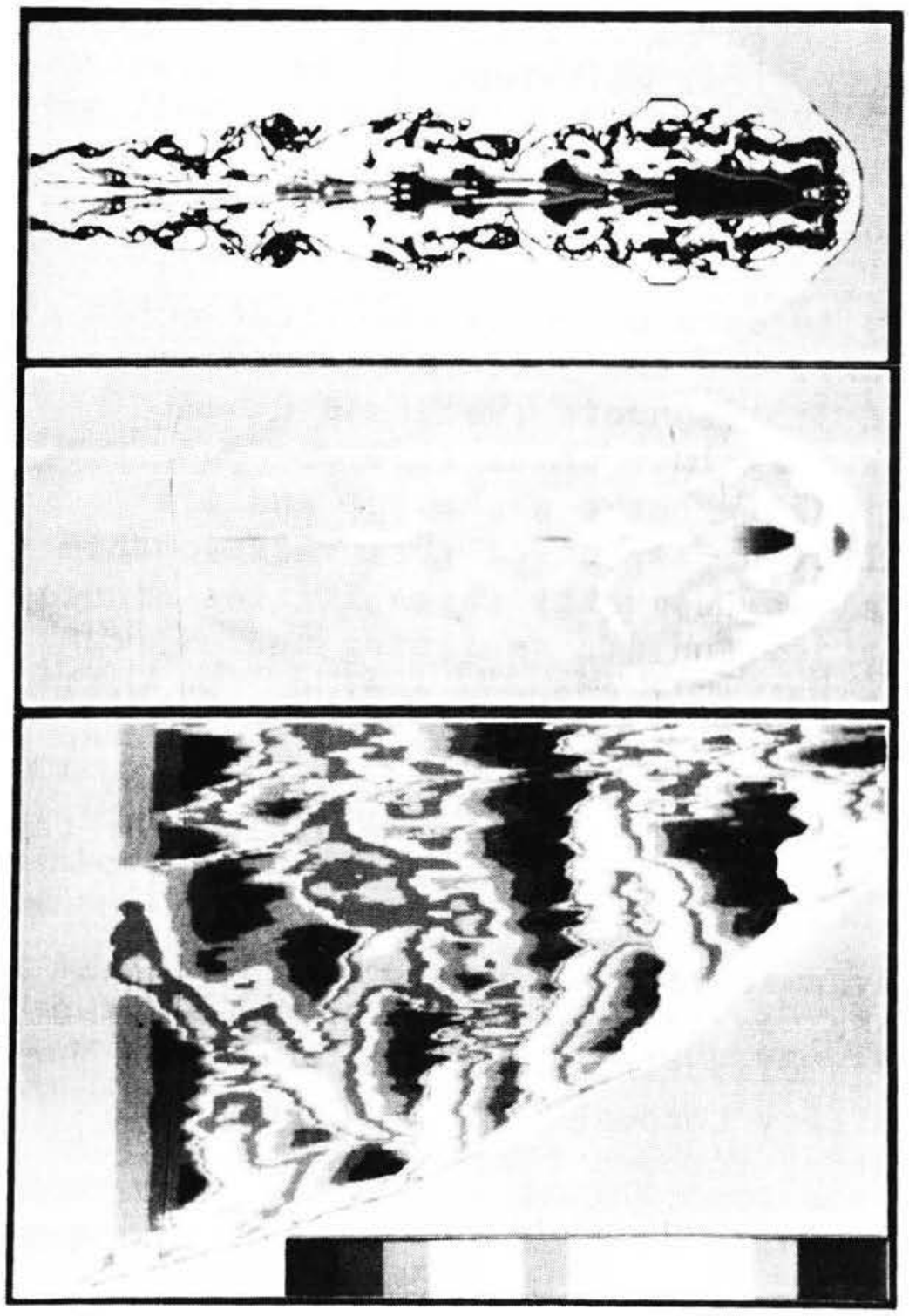


Plate 12. Density Ratio = 0.1, Mach Number = 12

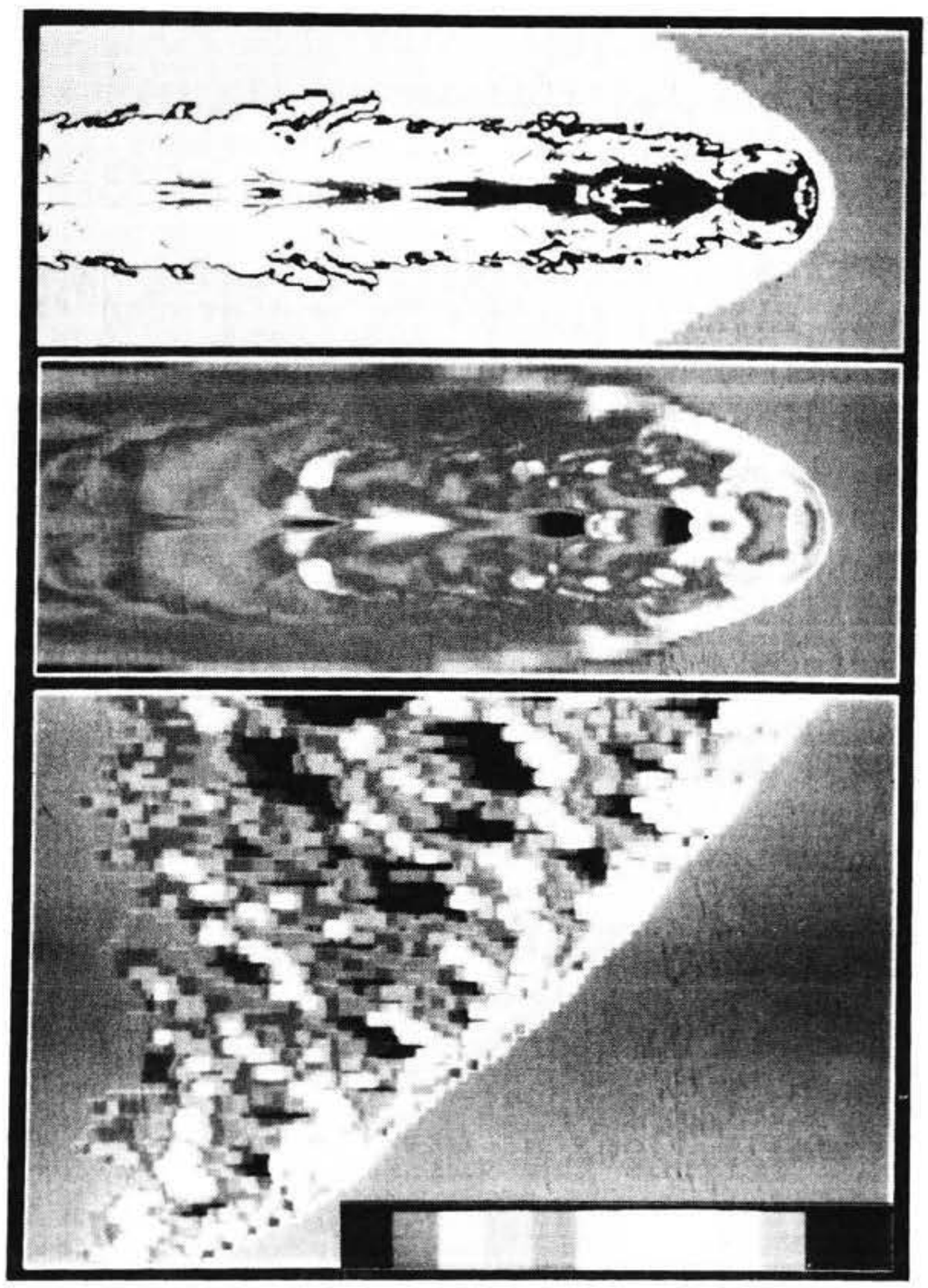


Plate 13. Density Ratio = 0.01, Mach Number = 12